Published in final edited form as:
Cell. 2008 October 3; 135(1): 97–109. doi:10.1016/j.cell.2008.08.017.

Mre11 Dimers Coordinate DNA End Bridging and Nuclease Processing in Double-Strand-Break Repair

R. Scott Williams[1,3,8], **Gabriel Moncalian**[1,3,8,7], **Jessica S. Williams**[1], **Yoshiki Yamada**[1], **Oliver Limbo**[1], **David S. Shin**[1,3], **Lynda M. Groocock**[1], **Dana Cahill**[4], **Chiharu Hitomi**[1,3], **Grant Guenther**[1], **Davide Moiani**[1,3], **James P. Carney**[4,6], **Paul Russell**[1,2,*], and **John A. Tainer**[1,3,5,**]

1*Department of Molecular Biology, The Scripps Research Institute, 10550 North Torrey Pines Rd., MB4, La Jolla, CA 92037, USA*

2*Department of Cell Biology, The Scripps Research Institute, 10550 North Torrey Pines Rd., MB4, La Jolla, CA 92037, USA*

3*Skaggs Institute for Chemical Biology, The Scripps Research Institute, 10550 North Torrey Pines Rd., MB4, La Jolla, CA 92037, USA*

4*The Radiation Oncology Research Laboratory, Department of Radiation Oncology, University of Maryland School of Medicine, Baltimore, Maryland 21201, USA*

5*Life Sciences Division, Department of Molecular Biology, Lawrence Berkeley National Laboratory, Berkeley, CA 94720*

SUMMARY

Mre11 forms the core of the multifunctional Mre11-Rad50-Nbs1 (MRN) complex that detects DNA double-strand breaks (DSBs), activates the ATM checkpoint kinase, and initiates homologous recombination (HR) repair of DSBs. To de?ne the roles of Mre11 in both DNA bridging and nucleolytic processing during initiation of DSB repair, we combined small-angle X-ray scattering (SAXS) and crystal structures of *Pyrococcus furiosus* Mre11 dimers bound to DNA with mutational analyses of ?ssion yeast Mre11. The Mre11 dimer adopts a four-lobed U-shaped structure that is critical for proper MRN complex assembly and for binding and aligning DNA ends. Further, mutations blocking Mre11 endonuclease activity impair cell survival after DSB induction without compromising MRN complex assembly or Mre11-dependant recruitment of Ctp1, an HR factor, to DSBs. These results show how Mre11 dimerization and nuclease activities initiate repair of DSBs and collapsed replication forks, as well as provide a molecular foundation for understanding cancer-causing Mre11 mutations in ataxia telangiectasia-like disorder (ATLD).

*Corresponding author, Paul Russell, E-mail: prussell@scripps.edu. **Corresponding author, John A. Tainer, E-mail: jat@scripps.edu.
[6]Current address – Battelle, Edgewood Chemical Biological Center, AMSRD-ECB-RT-BM, Bldg E3831, 5183 Blackhawk Road, Aberdeen Proving Ground, MD 21010
[7]Current address – Instituto de Biomedicina y Biotecnología de Cantabria, Santander, Spain.
[8]These authors contributed equally

Accession Numbers

Structures of the Mre11-synaptic DNA complex (PDB ID code 3DSC) and Mre11-branched DNA complex (PDB ID code 3DSD) are in the Protein Data Bank.

INTRODUCTION

DNA double-strand breaks (DSBs) are highly cytotoxic and genome-destabilizing DNA lesions. Mre11, the core subunit of the Mre11-Rad50-Nbs1 complex (Mre11 complex or MRN), plays central roles in DSB detection and repair. The importance of the Mre11 complex has been established in *Saccharomyces cerevisiae* and *Schizosaccharomyces pombe*, where it is critical for survival of DSBs induced by ionizing radiation (IR) and other genotoxins, as well as in humans, where hypomorphic mutations of *MRE11* and *NBS1* cause cancer-prone syndromes of ataxia telangiectasia-like disorder (ATLD) and Nijmegen breakage syndrome (NBS), respectively (Williams et al., 2007). ATLD and NBS cells exhibit cell cycle checkpoint defects, genome instability and IR hypersensitivity (Carney et al., 1998; Stewart et al., 1999).

As a DSB “first responder”, MRN recruits the ATM checkpoint kinase (yeast Tel1) (Lee and Paull, 2005) through binding to Nbs1 (Falck et al., 2005; You et al., 2005). ATM initiates a signaling cascade leading to cell cycle arrest and checkpoint responses key to genome integrity in humans, as evident from severe cancer predisposition and IR-sensitive phenotypes of ATM null patients (Shiloh, 2003). However, Mre11 complex subunits are essential for organism and cell viability in mammals, while ATM is not, so ATM recruitment and activation is only one of the important Mre11 complex functions.

One of the most interesting but least understood Mre11 complex activities is its DNA end sensing and DNA synaptic functions. Atomic force (AFM) (Chen et al., 2001; de Jager et al., 2001; Moreno-Herrero et al., 2005) and electron microscopic (EM) imaging (Hopfner et al., 2001; Hopfner et al., 2002) show MRN structurally segments into a globular DNA binding head, elongated mobile Rad50 coiled coils, and distal Rad50 hook domain. EM and AFM indicate DNA-bound heterotetrameric $Mre11_2Rad50_2$ (M_2R_2) bridges dsDNA ends via two arrangements. Simultaneous DNA binding within one M_2R_2 DNA binding head drives short-range bridging of DNA ends to within 100 Å of one another (Chen et al., 2001; Hopfner et al., 2002). Alternatively, reversible Zn^{2+}-dependant Rad50 hook domain assembly erects two-headed octameric $(M_2R_2)_2$ scaffolds to tether DNA chains up to 1200 Å apart (Moreno-Herrero et al., 2005). Biochemical studies suggest the DNA binding head bridges variable ends via the Mre11 protein, which interacts with ssDNA, dsDNA and forked DNA structures (Trenz et al., 2006; Wen et al., 2008). However, the basis for Mre11 complex DNA interactions is unknown due to an absence of high-resolution structures for any of the Mre11 complex components bound to DNA.

Another key and poorly understood Mre11 complex function is its role in nucleolytic processing of DNA ends. Mre11 has both ssDNA endonuclease and 3’–5’ exonuclease activities when assayed *in vitro*, but is paradoxically implicated in the 5’-3’ resection of DSBs *in vivo* (Williams et al., 2007). This resection generates a 3’ ssDNA tail, which is critical for DSB repair by homologous recombination (HR). Curiously, budding yeast studies show that mutations ablating Mre11 nuclease activities without destabilizing the complex cause mild IR sensitivity yet have strong effects in meiosis and cleavage of hairpin structures. These findings led to a prevailing view that Mre11 nuclease activity is not needed for DSB repair except in situations involving blocked DNA ends or unusual DNA structures (Bressan et al., 1998; Krogh et al., 2005; Lewis et al., 2004). Yet, structural and biochemical studies indicate that Mre11 is the core of the MRN complex DNA binding and processing head, participating in intermolecular interactions with itself, Rad50, Nbs1, and DNA substrates (Williams et al., 2007).

Here we integrate crystallographic, SAXS, and biochemical analyses of archaeal Mre11-DNA complexes with genetics in *S. pombe* to dissect the basis for Mre11 homodimerization, Mre11-DNA interactions, short-range Mre11-complex DNA synapsis, and Mre11 nucleolytic

mechanisms. Mre11-DNA complex structures allow the identification of single site mutants that retain Mre11 fold and interactions but ablate either exonuclease activity or both endonuclease and exonuclease activities. Furthermore, phenotypic analyses of single-site mutants in fission yeast establish that Mre11 dimerization and endonuclease activities are required for survival of DSBs. In agreement with characterizations of an Mre11 nuclease-dead mouse cell line in an accompanying paper (Buis et al., 2008), these findings show Mre11 nuclease activity is critical for DSB repair in both fission yeast and mammals.

RESULTS

Mre11-DNA Complex Structure Determination

As DSBs are induced by ionizing radiation and form when DNA replication forks encounter lesions (Wyman and Kanaar, 2006), they contain scission products with varied 5' or 3' overhanging ends, or ssDNA-dsDNA junctions generated by replication fork collapse. We therefore crystallized and determined X-ray structures of the catalytically active phosphoesterase domains (comprising the nuclease and nuclease-capping domains, residues 1–342) of *Pyrococcus furiosus* Mre11 bound to two distinct DNA oligonucleotide targets (see Experimental procedures, Figure 1 and Figure S1). The structures define two types of Mre11-DNA interactions: 1) a synaptic complex mimicking DNA end joining of products from a dsDNA scission event bearing a short 2bp 3' overhang (Figure 1A 1C and 1E) and, 2) a branched DNA structure that might be encountered by Mre11 at a collapsed fork (Figures 1B, 1D, and 1F). Two approaches promoted stabilization of nuclease-DNA complexes. For the synaptic end complex, we used EDTA to chelate divalent cations from the Mre11 active site. For the branched DNA complex, we used an H85S inactivating active site mutation (characterized herein) that does not alter active site Mn^{2+} binding, Mre11 stability, or macromolecular interactions. The synaptic end complex at 2.7 Å and branched complex at 2.2 Å resolution were phased by molecular replacement, fit to unbiased omit maps, and refined (Table S1).

Architecture of Mre11-DNA Complexes

To characterize Mre11-DNA assembly interfaces, we examined crystal packing and non-crystallographic symmetry interactions in the DNA-bound crystal forms. Both structures reveal a conserved four-helix bundle Mre11-Mre11 homodimeric interface. This interface at a two-fold axis in the C-centered orthorhombic unit cell in the synaptic complex (Figure 1C) matched that at the interface between non-crystallographic symmetry (NCS) related protomers in the branched DNA complex. A related interface in the DNA-free Mre11 structure was assumed to reflect crystal packing (Figure 1D) (Hopfner et al. 2001). These two DNA-bound structures imply this is the biologically relevant Mre11 dimer that interacts with diverse DNA substrates *in vivo*.

The dimer interface between helicies αB and αC of the Mre11 nuclease domain buries ~1400 $Å^2$ of solvent accessible surface area with van der Waals packing between hydrophobic residues Leu61, Ile65, Pro92, Leu97 and Phe101 (Figure 2A). The four-helix-bundle periphery is reinforced by a Lys62 to Asp100 intermolecular salt bridge, and capped near the basic DNA binding cleft by Arg55 side chain hydrogen bonding to an opposing Arg55 main chain carbonyl across the two-fold (synaptic end complex), or pseudo two-fold (branched complex) axis. Structure-based sequence alignments for human, yeast, and archaeal Mre11 homologues reveal that the high sequence identity amongst residues in this dimer interface is paralleled only by conservation within the five active site nuclease phosphoesterase motifs (Nuclease Motifs I–V) and DNA recognition loops (RL1–RL6) (Figure S1).

The U-shaped Mre11 dimer enables two subunits to simultaneously contact the dsDNA portions of the DNA substrates (Figure 1 and Figure 2). DNA makes extensive contacts to both

N-terminal calcineurin-like nuclease domains, and to a single C-terminal mixed α-β fold nuclease-capping domain (Figure 1A, 1B and Figure 2B–E). Core DNA contacts in the two complexes are analogous, but not equivalent (Figures 2B and 2C). Six DNA binding regions provide 17 residues for extensive DNA contacts in *cis* and in *trans* across the dimer. These six DNA recognition loops (RL1–RL6) converge into a contiguous DNA interaction surface (Figure 2B, 2C, 2D). DNA binding is mediated entirely by minor groove contacts to the sugar-phosphate backbone, explaining how Mre11 acts as a universal DNA processing enzyme (Figure 2E). For the large protein surface area (1525 $Å^2$) buried in the DNA interface, there is ~2:1 (500:275 $Å^2$ buried protein surface) distribution of DNA binding contacts for each subunit (Figure 2E). Mre11 dimerization is therefore key to efficient DNA binding.

Bound dsDNA is B-form with key deviations in overall and local helical parameters. Structural overlays of the synaptic complex DNA with a B-DNA template and analyses of helical parameters show that phosphate backbone and nucleotide conformation for base pair positions distal from the nuclease motifs (A4:T15, A5:T14, G6:C13, and C7:G12 base pairs, Figure 2D) have idealized values. Conversely, the sugar phosphate backbone proximal to the active site (base pairs C3:G16, A2:T17, C1:G18; Figure 2D) show a protein induced ~2 Å minor groove widening and helical axis distortion, coupled with a 10° bend towards the major groove. Salt bridging and van der Waals contacts from DNA recognition loops RL1 (residues Lys18 and Pro19), RL4 (residue Lys111), RL5 (residue Trp150) and RL6 (residues Tyr325 and Lys327) engage the 5' strand. The 3' end direction is steered by contacts from loops RL2 (His52, Arg55, and Ser57), RL1 (Tyr13, Glu14) and RL3 (Asn89). In concert, RL3 Arg90 and three RL1 residues (His17, Pro19, and Glu14) interrogate the DNA minor groove, forming a wedge that redirects and distorts the duplex backbone in the synaptic end and branching DNA complexes (Figure 2D). Recognition and sculpting of the structurally malleable fray of the duplex end provides a probable determinant of Mre11 DNA end recognition, DNA unwinding, 3'–5' nuclease, and 5'- micro-homology pairing Mre11 complex reaction activities.

All core DNA binding elements are conserved in human, *Xenopus*, *S. cerevisiae*, and *S. pombe* Mre11 homologs except RL3 (Figure S1). Conserved Arg and Lys residues at the RL2 C-terminal end, which lies adjacent to RL3, may substitute for these contacts in eukaryotic Mre11. These small differences may reflect the differential functional requirements of eukaryotic enzymes, whose catalytic activities are modulated by Nbs1/Xrs2 (Lee et al., 2003; Trujillo et al., 1998) and Ctp1/CtIP/Sae2 (Lengsfeld et al., 2007; Limbo et al., 2007; Sartori et al., 2007).

DNA Synapsis and Branched DNA Binding

The Mre11-DNA structures show how Mre11 dictates multiple DNA scaffolding functions. In the synaptic end complex, the 50 × 60 × 70 Å binding cleft houses two opposed DNA ends (Figures 1C and 1E). The DNA ends are tethered on a near parallel trajectory, with an offset of about one duplex width when viewed down the DNA helical axes. This linear bridging provides a molecular mechanism to tether DNA ends short distances (Chen et al., 2001; Hopfner et al., 2002) and explains Mre11 complex roles in DSB recognition and signaling events (Limbo et al., 2007; Lisby et al., 2004).

In the branched complex, the substrate ssDNA-dsDNA junction binds at the nuclease-capping domain interface, implicating the capping domain in ssDNA binding of branched DNA substrates (Figures 2C and 2F). Unlike the synaptic complex, the branched DNA binds asymmetrically across the dimer (Figure 1D). Capping domain movement occludes the second DNA binding site in the crystal. The 4-nucleotide 3' ssDNA tail is diverted tangentially away from the dsDNA helical axis, and makes non-specific contacts to a positively charged surface formed by RL6 and capping domain helix αH (Figures 2C and 2F). Three conserved basic residues (Lys318, Arg332, and Lys327) bind the phosphate backbone of the 3' end, and

intriguingly, sculpt the last three 3' nucleotides to adopt B-form conformation (Figure 2F). We therefore propose capping domain-DNA interactions can also participate in end-on dsDNA duplex binding such that the two interaction surfaces would simultaneously accommodate branched architectures of partially replicated collapsed replication forks. In combination, Mre11 dimer and capping domain DNA interactions shown in the crystal structures appear suitable to dictate multiple DNA tethering functions.

Mre11 Dimerization Facilitates DNA Binding

To examine roles of Mre11 dimerization in DNA binding and catalysis by the Mre11 complex in solution, we assessed Mre11 shape and oligomeric state using analytical gel filtration and small angle X-ray scattering (SAXS, Putnam et al., 2007) (Figure 3 and Figure S2). Experimental scattering curves for WT-Mre11 compared to calculated scattering from monomeric or dimeric Mre11 model structures reveals a close correspondence to the dimeric model, and a poor fit to the monomer profile (Figure 3E, Table S3). The calculated radius of gyration (R_g) derived from SAXS Guinier analysis (34.6 +/− 0.02 Å), the apparent molecular weight from analytical gel filtration (~74 kDa), and bimodal shape and maximum particle dimension (D_{max}= 120 Å) found in the SAXS electron pair distribution function (P(r)) all agree with the bi-lobed Mre11 crystal structures (Figure 3A, 3C and Figure S2; Table S2). Alignment of the dimeric crystal structure with averaged molecular envelopes from *ab initio* SAXS shape reconstruction further reveals the close agreement of the solution structures with the Mre11 crystallographic dimer assembly (Figure 3D).

To test if the four-helix bundle assembly mediates self-association, we introduced charged residue substitutions into the Mre11 hydrophobic dimer interface. Four closely associated conserved leucines are centered at the dimer core (Figure 3B). Mre11 harboring mutations of these leucines to charged residues (Mre11-L61K or Mre11-L97D) retain normal thermo-stability at 65 °C, but migrate as significantly smaller (~36kDa apparent MW) protein species in gel filtration (Figure 3A; Table S2). SAXS analysis shows that Mre11-L61K and Mre11-L97D are converted to smaller forms with distinct skewed mono-modal P(r) functions and a significantly smaller D_{max} values (~85–90 Å) compared to wild type Mre11 (Figures 3C). While the gel filtration analysis with proteins at ~12.5 μM concentration shows effective disruption of stable Mre11 dimerization by mutation of the hydrophobic interface, SAXS solution scattering data for dimer mutants at high concentration (250 μM) is best fit using a mixed monomer/dimer equilibrium model (Figure S2 and Table S3). Thus dimerization is mediated via a conserved hydrophobic four-helix bundle, and introduction of positive and negative charge into this interface disrupts the dimer.

To probe the functional importance of dimerization, we used EMSA analysis of DNA binding and measured nucleolytic activities of dimer variants. Wild type Mre11 binds 40-mer ssDNA with high affinity (K_d = 170 nM) and has a ~6.5-fold lower affinity on for 40 bp dsDNA (K_d = 1.1 μM) (Figure 3F and Figure S3). By contrast, the monomeric Mre11-L61K and Mre11-L97D dimer mutants that lose ~1/3 of their total DNA contact surface show 30 to >50 fold decreased affinity for ssDNA, and a 3 to >10 fold decreased affinity for dsDNA. Mre11-L61K and Mre11-L97D retain high levels of ssDNA endonuclease activity (Figure 3G) and 3'–5' dsDNA exonuclease activity (not shown), suggesting a high-affinity DNA interaction across the dimeric interface is not essential for efficient exo- and endonucleolytic catalysis. These results dissect Mre11 catalytic and architectural functions. Mre11 dimerization is not critical for catalysis but may enable architectural DNA binding functions of MRN by promoting high affinity DNA interactions. Specifically, our SAXS and X-ray crystal structures suggest that the Mre11 dimer characterized here is the core of the Mre11 complex DNA binding head that recognizes diverse DNA structures and promotes of short range DNA synapsis.

Mre11 3'–5' Exonuclease Mechanism

To test the structural implications of the DNA complexes for the Mre11 exonuclease polarity and dissect determinants of exo- and endonucleolytic catalysis, we examined the trajectories of the 3' ends of the bound dsDNAs. In both Mre11-DNA complexes, the 3' termini trace a path along the DNA binding cleft towards the active site, consistent with reported 3'–5' dsDNA exonuclease directionality, and the orientation of 5'-dAMP nucleolytic product binding (Figures 1E and 1F) (Hopfner et al., 2001; Paull and Gellert, 1998). These structures support a three step 3'–5' nuclease mechanism (Figure 4A): 1) DNA binding, 2) duplex melting linked to capping domain rotation, 3) phosphate rotation and nucleolysis driven by conserved nuclease motif II and motif III histidines His52/His85.

In the two complexes, DNA duplexes occupy similar, but non-equivalent positions and registers in the binding cleft (Figure 4C). Structural overlays indicate DNA translocation is linked to capping domain rotation, reorientation of the Mre11 dimerization axis, and movement of the RL1 minor groove wedge (Figure 4C). Thus, following an initial DNA interaction, capping domain rotation and associated plastic deformations may drive duplex end melting. A relay of van der Waals contacts initiated by the capping domain and involving residues Phe16, Lys18, His17, Tyr301, and Tyr325 advances the RL1 wedge into the DNA minor groove (Figure 4C). The net result of these movements is a ~2/3 base pair step helical translocation towards the active site, and disruption of terminal base pairing interactions, as visualized for the synaptic complex DNA, where the wedge penetrates further into the minor groove (Figure 4D). Consistent with this model, a wedge component mutant (H17A) exhibits a 30–35% reduction in 3'–5' exonuclease activity, as monitored by release of the fluorescent adenine analog 2-aminopurine from the 3' end of a preferred Mre11 blunt dsDNA exonuclease substrate (Figure 4B). Thus, the capping domain rotation may govern the ATP hydrolysis-independent dsDNA unwinded by Mre11 complex (Paull and Gellert, 1999). Interestingly, *P. furiosus* Mre11 is ~12-fold less active on a branched substrate (Figure S4). Stable 3' end binding by the capping domain with limited exonucleolysis or endonucleolysis may ensure maintenance and control of the integrity of recombinogenic DNA 3' termini.

Base pair melting and minor groove widening helps accommodate DNA backbone access requirement for exonucleolytic activity on preferred blunt or 3' recessed dsDNA substrates. Based upon the positions of the DNA 3' termini in the Mn^{2+} bound and unbound structures (Figure 4D - grey 3' terminus), the 3' end trajectory (Figure 4C- yellow 3' terminus) is evident from bound 5'-dAMP in the exonuclease product structure (Hopfner et al., 2001). Following duplex melting, phosphate rotation three base pairs 5' to the cleavage site would redirect the 3' terminus into the active site cleft for cleavage. Two stringently conserved histidines (motif II His52 and motif III His85) gate the 3' end path to the product-binding site (Figure 4D). Except His52 and His85, most residues from nuclease motifs I–V act directly in metal ion binding and active site assembly. His52 and His85 are unique in being removed from the Mn^{2+} ligands: the Mre11-H85S ternary complex structure with bound Mn^{2+} and branched DNA substrate shows His85 mutation does not influence Mn^{2} occupancy (Figure S5).

Conserved Mre11 Motifs Regulating Structure-Specific Nuclease Activities

To test our catalytic model, we examined His52 and His85 roles in 3'–5' exonucleolytic and ssDNA endonucleolytic cleavage. H52S and H85S mutants lack 3'–5' exonuclease activity (Figure 4B). His85 binds the 5'-dAMP phosphate with an implied role in stabilizing the penta-covalent transition state during hydrolysis (Hopfner et al., 2001), but His52 was proposed to act in a charge relay with His85 during transition state stabilization (Hopfner et al., 2001). Here, His52 interactions with the phosphate backbone suggest this motif II histidine acts in phosphate rotation (Figure 4D and Figure S5). So, our data implicate distinct critical roles for

His52 and His85, with motif II His52 driving phosphate rotation for 3'–5' exonucleolytic activity.

DNA docking analyses suggests ssDNA may approach the active site by an alternative binding mode (Figure 4F). Also as ssDNA is flexible, we hypothesized ssDNA endonucleolytic cleavage should not require Motif II His52 phosphate rotation function to access the DNA backbone, but should require di-Mn ion directed alignment of the scissile phosphodiester bond, and transition state stabilization by Motif III His85. As predicted, the H85S mutant lacks endonuclease activity, while H52S displays only slightly diminished endonucleolytic cleavage of circular ϕX174 ssDNA (Figure 4E). These results suggest dsDNA exonuclease and ssDNA endonuclease activities have distinct, structure-specific, DNA-alignment requirements for nucleolytic cleavage (Figures 4G and 4H). Motif II mutation H52S ablates 3'–5' exonuclease activity, but retains endonuclease activity. In contrast, disruption of Motif III histidine His85 blocks both Mre11 endonuclease and 3'–5' exonuclease activities.

DSB Repair Functions Require Mre11 Dimerization and Endonucleolytic Activities

Guided by the *P. furiosus* Mre11-DNA complex structures, we made mutant alleles of *S. pombe mre11* (*rad32*) to test if Mre11 dimerization and nucleolytic activities are required for DSB repair. We analyzed two classes of mutations: 1) dimerization mutations deficient in DNA binding that retain exonuclease and endonuclease activities, and 2) catalytically-deficient mutants that segregate exonucleolytic and endonucleolytic activities, but do not alter metal coordination or Mre11 complex formation.

To probe the Mre11-Mre11 interface, we substituted charged residues for Leu77 and Leu154 in *S. pombe* Mre11 (*P. furiosus* Mre11 Leu61 and Leu97; Figure S1). Two-hybrid analyses shows that wild type Mre11 had a robust self-interaction, but mutations of dimer interface leucines severely diminished interactions (Figure 5A, upper panels). Importantly, these mutations did not impair interactions with Rad50 and Nbs1 (Figure 5C, upper panel). We reasoned that while charged residue substitutions blocked the Mre11 self-interaction, the interface might be re-engineered to associate via a salt bridging network that occupied a similar volume (Figure 5B). This charge-restored interface design tests the need for the specific interface versus another direct connection. Replacement of the LL/LL hydrophobic interface with a KD/KD or DK/DK salt-bridging network partially restored the interaction, as measured by two-hybrid (Figure 5A, lower panels). However, while the monomeric single variants L77K and L154D interact with Nbs1 and Rad50, the salt-bridge L77K/L154D dimer is defective in these interactions (Figure 5C). Thus, precise Mre11 dimer assembly, consistent with DNA-binding and end-pairing geometries observed in our Mre11-DNA complex crystal structures, is critical for a functional Mre11 complex.

To test if dimerization mutants are sensitive to genotoxins, we examined responses to four damaging agents: 1) ionizing radiation (IR), which directly makes DSBs, 2) UV light, which creates DNA photoproducts that can be processed into DSBs, 3) camptothecin (CPT), a topoisomerase inhibitor, which causes replication fork breakage when the replisome encounters a topoisomerase-CPT complex, and 4) hydroxyurea (HU), which stalls replication forks by inhibiting ribonucleotide reductase, an enzyme required for dNTP synthesis. The *mre11* alleles replace genomic *mre11*$^{+}$ and encode a C-terminal myc tag. These strains were compared to *mre11Δ* and to a myc-tagged *mre11*$^{+}$ strain, which appeared identical to untagged *mre11*$^{+}$ in survival assays (Figures 5D and 5E). Immunoblotting showed that the *L77K* and *L154D* mutants express at levels comparable to wild type, whereas *L77K/L154D* abundance was reduced ~50%.

Consistent with its poor ability to interact with Rad50 and Nbs1 in yeast two-hybrid assays, the *L77K/L154D* double mutant resembled *mre11Δ* in being very sensitive to genotoxins,

(Figures 5D and 5E). The *L154D* mutant was sensitive to the higher dose (2 mM) of CPT but was otherwise largely genotoxin insensitive. Yet, *L77K* was sensitive to all the genotoxins and most notably to CPT, but less so than *mre11Δ*. These data show that the dimer interface is important for Mre11 DSB repair function. The mild defect for L154D and intermediate defect of the *L77K* mutant suggest that the mutations do not fully disrupt Mre11 dimerization in vivo or that ablating dimerization does not fully inactivate Mre11. Although *S. pombe* Mre11 dimer mutant variants may not interact in isolation (Figure 5A), upon binding to dimeric Rad50, the increased Mre11 local concentration may enable association of reduced-affinity dimers, as seen for the *P. furiosus* Mre11 dimer mutants. Intriguingly, Mre11 ATLD missense variants (hMre11 N117S and W210C) also disrupt Nbs1 interactions (Fernet et al. 2005; Lee et al, 2003; Stewart et al., 1999) and map to one surface on the Mre11 dimer removed from the DNA binding cleft (Figure 5F). Thus Mre11 ATLD mutations and dimer mutants resulting in subunit misalignment may both impact protein-protein interactions by distorting the Mre11 surface, and are analogous to cancer-causing XPD mutations distorting domain interfaces (Fan et al., 2008), and BRCA1 mutants that ablate protein-phosphopeptide binding surfaces (Williams et al. 2004).

To test roles of the exonucleolytic and endonucleolytic activities in fission yeast, we employed the phosphate rotation motif II mutation (*H68S*, corresponding to *P. furiosus mre11-H52S*), and the nuclease transition state stabilization motif III mutation (*H134S*, corresponding to *P. furiosus mre11-H85S*). Both mutants displayed robust two-hybrid self-interactions, indicating that they do not impair Mre11 dimerization (Figure 5A). Likewise, both mutants strongly interacted with Rad50 and Nbs1 (Figure 5C). Immunoblotting showed that they were present at levels similar to wild type Mre11 in *S. pombe* (Figure 5E). Remarkably, the *H68S* mutant, which is expected to be severely deficient in 3'–5' exonuclease activity while maintaining endonuclease activities, showed only mild CPT and IR sensitivity at high doses. In contrast, the *H134S* mutant, that is expected to lack all nuclease activities, showed genotoxin sensitivity approaching *mre11Δ* (Figures 5D and 5E). As Mre11 is required for HR, but not NHEJ repair in fission yeast (Manolis et al., 2001), nuclease activity is important for Mre11 function in DSB repair, and this is most probably endonuclease activity (Figure 5G).

Exo1 Rescues *mre11-H134S*

As the nuclease-deficient *mre11-H134S* is highly sensitive to genotoxins, we examined whether these phenotypes show defects in processing DNA ends and whether they may be linked to Ctp1, a critical co-factor for MRN 5’ to 3’ resection function (Limbo et al., 2007). Mre11 and Ctp1 deficiency are partially suppressed by elimination of the Ku80 subunit of the Ku70-Ku80 DNA end-binding complex that promotes NHEJ and protects DNA ends from the 5’ to 3’ resection activity of Exo1 exonuclease (Limbo et al., 2007; Tomita et al., 2003). A *pku80Δ* mutation suppressed the slow growth phenotype, IR, CPT and UV sensitivities of *mre11-H134S* cells (Figure 6A). Importantly, the extreme genotoxin sensitivity of the *mre11-H134S pku80Δ exo1Δ* strain showed that this suppression was dependent on Exo1 activity. Indeed, the *exo1Δ* mutation substantially exacerbated the *mre11-H134S* phenotypes. Similar genetic interactions are seen in *S. cerevisiae*, although the double mutant phenotype is mild compared to *mre11Δ* (Moreau et al., 2001). The ability of Exo1 to suppress *mre11-H134S* strongly suggests that the *mre11-H134S* phenotypes reflect an inability to properly resect DSBs.

As Ctp1 is required for the MRN-dependent processing of DSBs, and Mre11 is required for localization of Ctp1 at DSBs (Limbo et al., 2007), it was important to establish if the *mre11-H134S* phenotype might be a Ctp1 recruitment defect. We therefore used a chromatin immunoprecipitation (ChIP) experiment to determine if *mre11-H134S* cells recruit Ctp1 to a DSB created by HO endonuclease. This analysis detected robust enrichment of Mre11-H134S,

Nbs1 and Ctp1 to a region 0.2 kb from the DSB (Figures 6B and 6C). As seen before (Limbo et al., 2007), phosphorylation of histone H2A (γ-H2A) was detected a regions further from the DSB (2–16 kb), but not 0.2 kb from the DSB site. These data show that the H134S mutation does not interfere with the Mre11 association with DSBs, nor does it impair recruitment of Nbs1 or Ctp1. Therefore, *mre11-H134S* defects likely reflect specific impairment of Mre11 endonuclease.

DISCUSSION

Consistent with our EM (Hopfner et al. 2001) and X-ray structures, AFM shows hetero-trimeric yeast Mre11-Rad50-Xrs2 complexes tether chains of 400–500bp dsDNA into concatamers with the globular DNA binding head localized at the junction of linearly joined DNA repeats (Chen et al., 2001). Mre11-DNA structures further uncover how the Mre11 dimer is tailored to recognize and bridge the diverse DNA architectures encountered at breaks or ssDNA-dsDNA junctions, such as collapsed or restarting replication forks (Costanzo et al., 2001; Trenz et al., 2006; Wen et. al., 2008). These results explain and extend observations that the Mre11 complex forms DNA damage repair nuclear foci upon replication fork collapse in budding yeast (Lisby et al., 2004), prevents accumulation of DSBs during replication in Xenopus extracts (Costanzo et al., 2001; Trenz et al., 2006), and is an early sensor of IR (Mirzoeva and Petrini, 2001) or endonuclease-induced DSBs (Lisby et al., 2004). Thus, the Mre11 complex harbors adaptable and multivalent DNA bridging capabilities, and utilizes distinct modes of long-range and short-range DNA tethering to sense, coordinate, process, and port variable DNA ends to HR repair proteins (Figure 7).

Active site mutations dissect the functional relevance of Mre11 nuclease activities in DSB repair. The mild phenotypes displayed for the *S. pombe* phosphate rotation *H68S* mutant suggest that a robust Mre11 3'–5' exonuclease activity is not critical for HR repair. In contrast, the transition state stabilization *H134S* mutant is nearly as sensitive to clastogens as the Mre11 null mutation, suggesting that Mre11 endonuclease activity is crucial for HR repair of DSBs, although 3'–5' exonuclease activity may aid resection. The *H134S* mutation is a nucleolytic defect because this protein maintains robust interactions with metal co-factors, Rad50, and, Nbs1, and mediates Nbs1 and Ctp1 recruitment to DSBs.

The *mre11-H134S* mutation's strong phenotype in fission yeast contrasts with similar budding yeast *mre11* mutants, which show mild IR sensitivity (Krogh et al., 2005; Lewis et al., 2004). Yet, an analogous murine Mre11-H129N allele maintains Nbs1 and Rad50 interactions, but shows impaired recruitment of RPA and Rad51 into ionizing radiation induced nuclear foci and a 90% reduction in HR repair efficiency, consistent with our genetic data suggesting a 5'–3' resection defect for S. *pombe Mre11-H134S*. Moreover, Mre11-H129N also confers early embryonic lethality in mouse, and conditional knock-in of this allele causes severe IR hypersensitivity (Buis et al., 2008).

We therefore propose that Mre11 endonuclease activity acts in conjunction with additional factors that open DNA ends to produce an effective 5'-3' excision process that liberates 3' ssDNA for RPA loading and initiation of strand invasion in early HR repair steps *in vivo*. This function is likely mediated by the eukaryotic Ctp1 (CtIP) protein, which is required for HR repair in *S. pombe* and human cells, and modifies the human Mre11 complex endonuclease activity *in vitro* (Limbo et al., 2007; Sartori et al., 2007). Ctp1 (CtIP) is a probable ortholog of budding yeast Sae2, which has a hairpin nicking activity *in vitro* (Lengsfeld et al., 2007). Interestingly, budding yeast *sae2Δ* mutants have a mild IR-sensitive phenotype (Rattray et al., 2001) similar to the *mre11-H125N* or *H125S* nuclease mutations, whereas fission yeast *ctp1Δ* mutants have a more severe IR-sensitive phenotype equivalent (Limbo et al, 2007). These

differences may reflect that budding yeast MRX has acquired additional nuclease-independent NHEJ functions.

Our combined observations suggest Mre11 is crucial for sensing, processing and coordinating control of both ssDNA and dsDNA during HR repair. Mre11 endonucleolytic cleavage of ssDNA and regions neighboring transiently formed secondary structures contributes to the 5'-3' resection processing reaction (Figure S6) (Trujillo and Sung, 2001). By contrast, the Mre11 3'–5' exonuclease is well suited for Mre11 complex roles in 5'-microhomology mediated end-joining pathways (Figure S7) (Paull and Gellert, 1998; Paull and Gellert, 2000). Employment of two juxtaposed DNA binding clefts may help validate repair status by sensing an empty DNA binding cleft, versus one or two bound DNA ends. Furthermore, as seen for the FEN-1 complex with dsDNA (Chapados et al., 2004), controlling the 3' primer terminus at a strand break may be a critical function for the Mre11 complex. Together, these results highlight the Mre11 structural and enzymatic contributions within the DSB repair complex to the biological needs for both creating and controlling proper 3'-OH ends to prime DNA repair synthesis.

EXPERIMENTAL PROCEDURES

Protein Expression and Purification

Expression and purification of wild type and mutant *P. furiosus* Mre11 (residues 1–342) followed published procedures (Hopfner et al., 2001). The H52S, H52S, L77K and L97D mutants were introduced by Quickchange (Stratagene).

Crystallization, X-ray Diffraction Data Collection, Structure Determination and Refinement

We employed four-thymine hairpin DNA architectures to promote directional binding of duplex ends during crystallization (Figure S8). For the synaptic complex, Mre11 (at 30 mg/ml in 200 mM NaCl, 20 mM TrisHCl, pH 7.5, 1mM DTT and 0.5 mM EDTA) and DNA substrate (5'-CAC AAG CTT TTG CTT GTG AC-3') were mixed at a 3:1 DNA:protein molar ratio. Complex crystals (space group C222) were grown with sitting drop vapor diffusion at 20–22 °C by mixing 1 μl Mre11-DNA complex with 1 μl reservoir solution 1 (20% polyethylene glycol 1000, 0.1 M Tris-HCl pH 7.5, 0.2 M magnesium chloride, 0.2 M 1,6 hexanediol). Data to 2.7 Å were collected at 105 °K from a crystal transferred to cryoprotectant solution 1 (20 % (v/v) ethylene glycol, 16 % PEG1000, 0.08 M Tris-Cl pH 7.5, 0.16 M magnesium chloride, 0.16 M 1,6 hexanediol).

For the Mre11-His85Ser/Mn^{2+}/Branched-DNA ternary complex, Mre11-H85S (at 10mg/mL in 100 mM NaCl, 20mM Tris HCl 7.5) was mixed at a 3:1 DNA:protein ratio with the branched oligonucleotide hairpin (5'-CGC GCA CAA GCT TTT GCT TGT GGA TA-3') 30 min. before crystallization. By hanging drop vapor diffusion at 22°C, orthorhombic crystals (space group $P2_12_12_1$) grew within one week following mixing 1 μl complex with 1 μl reservoir solution 2 (40% v/v Polyethylene glycol 200, 100mM HEPES pH 7.5). Crystals were flash cooled in liquid nitrogen directly from hanging drops and diffraction data was collected to 2.2 Å (See Table S1).

Data processing, phasing, model building and refinement are detailed in the Supplemental data. Final refined models of the synaptic complex at 2.7 Å (R/R_{free} = 22.8/27.8) and branched complex at 2.2 Å (R/R_{free} = 20.0/24.6) exhibit good geometric parameters (Table S1).

Small Angle X-ray Scattering (SAXS)

SAXS data for wild type PfMre11 catalytic domain and dimerization mutants (PfMre11-L61K, L97D) were acquired at the Advanced Light Source SIBYLS beamline (BL12.3.1). 15μL samples in a 1mm thick sample cell equipped with 25 uM Mica windows at a sample to detector

distance of 1.5m were illuminated at 10 keV (λ=1.1159 Å) for data collection (q-range = 0.010 $Å^{-1}$ - 0.250 $Å^{-1}$). Scattering profiles in SAXS buffer (500 mM NaCl, 20mM Tris 7.5, 5% glycerol, 1mM DTT) were collected from 10 mg/mL samples and analyzed (see Supplemental Data).

Nuclease and Electrophoretic Mobility Shift Assays

Mre11 exonuclease and endonuclease assays were performed as described (Hopfner et al., 2001) using substrates detailed in the Supplemental data. DNA binding reactions for EMSAs were carried out in 25 mM HEPES pH= 8.0, 50 mM NaCl, 1 mM DTT, 0.1 μg/μl acetylated bovine serum albumin, 10% glycerol containing 50 fmol of DNA substrates (see Supplemental data).

Strain Construction, plate Survival, Yeast two-hybrid, and HO ChIP Assays

Plate and IR survival assays were performed as described (Limbo et al 2007) for strains described in the Supplemental Data. Two hybrid assays were performed as previously described (Limbo et al 2007). Chromatin immunoprecipitation assays were conducted as described previously (Limbo et al 2007).

Immunoblotting

Whole cell extracts were prepared from exponentially growing cells. Cells were lysed in 0.5% β-mercaptoethanol and 0.3M NaOH, protein was precipitated in 25% trichloroacetic acid, resuspended in SDS-PAGE sample buffer and incubated at 65°C for 15 min. Western blotting was performed using anti-Myc (9E10; Santa Cruz Biotechnology) and pstair (Sigma) antibodies.

Supplementary Material

Refer to Web version on PubMed Central for supplementary material.

ACKNOWLEDGEMENTS

R.S.W. is supported by the Canadian Institutes of Health Research, the Alberta Heritage Foundation for Medical Research, and the Skaggs Institute for Chemical Biology fellowships. Y.Y. is supported by a Uehara Memorial Foundation fellowship. Work on the Mre11 complex in the authors' laboratories is supported in part by National Cancer Institute grants CA117638, CA92584 and CA77325. Lawrence Berkeley National Laboratory efforts are supported in part by U.S. Department of Energy programs IDAT (for Integrating crystallography and X-ray scattering) and MAGGIE (for defining Pyrococus complexes) under Contract Number DE-AC02-05CH11231. We thank Scott Classen, Michal Hammel, Greg Hura and Susan Tsutakawa for assistance with SAXS and X-ray data collection at the Advanced Light Source SIBYLS beamline, and Brian Chapados for discussions and comments.

REFERENCES

Bressan DA, Olivares HA, Nelms BE, Petrini JH. Alteration of N-terminal phosphoesterase signature motifs inactivates Saccharomyces cerevisiae Mre11. Genetics 1998;150:591–600. [PubMed: 9755192]

Buis J, Wu Y, Deng Y, Leddon J, Westfield G, Eckersdorff M, Sekiguchi JM, Chang S, Ferguson DO. Mre11 Nuclease activity has essential roles in DNA repair and genomicstability distinct from ATM activation. Cell. 2008xxxxx

Carney JP, Maser RS, Olivares H, Davis EM, Le Beau M, Yates JR 3rd, Hays L, Morgan WF, Petrini JH. The hMre11/hRad50 protein complex and Nijmegen breakage syndrome: linkage of double-strand break repair to the cellular DNA damage response. Cell 1998;93:477–486. [PubMed: 9590181]

Chahwan C, Nakamura TM, Sivakumar S, Russell P, Rhind N. The fission yeast Rad32 (Mre11)-Rad50-Nbs1 complex is required for the S-phase DNA damage checkpoint. Mol Cell Biol 2003;23:6564–6573. [PubMed: 12944482]

Chapados BR, Hosfield DJ, Han S, Qiu J, Yelent B, Shen B, Tainer JA. Structural basis for FEN-1 substrate specificity and PCNA-mediated activation in DNA replication and repair. Cell 2004;116:39–50. [PubMed: 14718165]

Chen L, Trujillo K, Ramos W, Sung P, Tomkinson AE. Promotion of Dnl4-catalyzed DNA end-joining by the Rad50/Mre11/Xrs2 and Hdf1/Hdf2 complexes. Mol Cell 2001;8:1105–1115. [PubMed: 11741545]

Costanzo V, Robertson K, Bibikova M, Kim E, Grieco D, Gottesman M, Carroll D, Gautier J. Mre11 protein complex prevents double-strand break accumulation during chromosomal DNA replication. Mol Cell 2001;8:137–147. [PubMed: 11511367]

de Jager M, van Noort J, van Gent DC, Dekker C, Kanaar R, Wyman C. Human Rad50/Mre11 is a flexible complex that can tether NA ends. Mol Cell 2001;8:1129–1135. [PubMed: 11741547]

Falck J, Coates J, Jackson SP. Conserved modes of recruitment of ATM, ATR and DNA-PKcs to sites of DNA damage. Nature 2005;434:605–611. [PubMed: 15758953]

Fan L, Fuss JO, Cheng QJ, Arvai AS, Hammel M, Roberts VA, Cooper PK, Tainer JA. XPD Helicase Structures and Activities Provide Insights into Cancer and Aging Phenotypes from XPD Mutations. Cell 2008;133:789–800. [PubMed: 18510924]

Fernet M, Gribaa M, Salih MA, Seidahmed MZ, Hall J, Koenig M. Indentification and functional consequences of a novel Mre11 mutation affecting 10 Saudi Arabian patients with the ataxia telangiectasia-like disorder. Hum Mol Genet 2005;14:307–318. [PubMed: 15574463]

Hopfner KP, Karcher A, Craig L, Woo TT, Carney JP, Tainer JA. Structural biochemistry and interaction architecture of the DNA double-strand break repair Mre11 nuclease and Rad50-ATPase. Cell 2001;105:473–485. [PubMed: 11371344]

Hopfner KP, Craig L, Moncalian G, Zinkel RA, Usui T, Owen BA, Karcher A, Henderson B, Bodmer JL, McMurray CT, et al. The Rad50 zinc-hook is a structure joining Mre11 complexes in DNA recombination and repair. Nature 2002;418:562–566. [PubMed: 12152085]

Krogh BO, Llorente B, Lam A, Symington LS. Mutations in Mre11 phosphoesterase motif I that impair Saccharomyces cerevisiae Mre11-Rad50-Xrs2 complex stability in addition to nuclease activity. Genetics 2005;171:1561–1570. [PubMed: 16143598]

Lee JH, Ghirlando R, Bhaskara V, Hoffmeyer MR, Gu J, Paull TT. Regulation of Mre11/Rad50 by Nbs1: effects on nucleotide-dependent DNA binding and association with ataxia-telangiectasia-like disorder mutant complexes. J Biol Chem 2003;278:45171–45181. [PubMed: 12966088]

Lee JH, Paull TT. ATM activation by DNA double-strand breaks through the Mre11-Rad50-Nbs1 complex. Science 2005;308:551–554. [PubMed: 15790808]

Lengsfeld BM, Rattray AJ, Bhaskara V, Ghirlando R, Paull TT. Sae2 is an endonuclease that processes hairpin DNA cooperatively with the Mre11/Rad50/Xrs2 complex. Mol Cell 2007;28:638–651. [PubMed: 18042458]

Lewis LK, Storici F, Van Komen S, Calero S, Sung P, Resnick MA. Role of the nuclease activity of Saccharomyces cerevisiae Mre11 in repair of DNA double-strand breaks in mitotic cells. Genetics 2004;166:1701–1713. [PubMed: 15126391]

Limbo O, Chahwan C, Yamada Y, de Bruin RA, Wittenberg C, Russell P. Ctp1 is a cell-cycle-regulated protein that functions with Mre11 complex to control double-strand break repair by homologous recombination. Mol Cell 2007;28:134–146. [PubMed: 17936710]

Lisby M, Barlow JH, Burgess RC, Rothstein R. Choreography of the DNA damage response: spatiotemporal relationships among checkpoint and repair proteins. Cell 2004;118:699–713. [PubMed: 15369670]

Manolis KG, Nimmo ER, Hartsuiker E, Carr AM, Jeggo PA, Allshire RC. Novel functional requirements for non-homologous DNA end joining in Schizosaccharomyces pombe. Embo J 2001;20:210–221. [PubMed: 11226171]

Mirzoeva OK, Petrini JH. DNA damage-dependent nuclear dynamics of the Mre11 complex. Mol Cell Biol 2001;21:281–288. [PubMed: 11113202]

Moreno-Herrero F, de Jager M, Dekker NH, Kanaar R, Wyman C, Dekker C. Mesoscale conformational changes in the DNA-repair complex Rad50/Mre11/Nbs1 upon binding DNA. Nature 2005;437:440–443. [PubMed: 16163361]

Moreau S, Morgan EA, Symington LS. Overlapping functions of the Saccharomyces cerevisiae Mre11, Exo1 and Rad27 nucleases in DNA metabolism. Genetics 2001;159:1423–1433. [PubMed: 11779786]

Paull TT, Gellert M. The 3' to 5' exonuclease activity of Mre 11 facilitates repair of DNA double-strand breaks. Mol Cell 1998;1:969–979. [PubMed: 9651580]

Paull TT, Gellert M. Nbs1 potentiates ATP-driven DNA unwinding and endonuclease cleavage by the Mre11/Rad50 complex. Genes Dev 1999;13:1276–1288. [PubMed: 10346816]

Paull TT, Gellert M. A mechanistic basis for Mre11-directed DNA joining at microhomologies. Proc Natl Acad Sci U S A 2000;97:6409–6414. [PubMed: 10823903]

Putnam CD, Hammel M, Hura GL, Tainer JA. X-ray solution scattering (SAXS) combined with crystallography and computation: defining accurate macromolecular structures, conformations and assemblies in solution. Q Rev Biophys 2007;40:191–285. [PubMed: 18078545]

Rattray AJ, McGill CB, Shafer BK, Strathern JN. Fidelity of mitotic double-strand-break repair in Saccharomyces cerevisiae: a role for SAE2/COM1. Genetics 2001;158:109–122. [PubMed: 11333222]

Sartori AA, Lukas C, Coates J, Mistrik M, Fu S, Bartek J, Baer R, Lukas J, Jackson SP. Human CtIP promotes DNA end resection. Nature 2007;450:509–514. [PubMed: 17965729]

Shiloh Y. ATM and related protein kinases: safeguarding genome integrity. Nat Rev Cancer 2003;3:155–168. [PubMed: 12612651]

Stewart GS, Maser RS, Stankovic T, Bressan DA, Kaplan MI, Jaspers NG, Raams A, Byrd PJ, Petrini JH, Taylor AM. The DNA double-strand break repair gene hMRE11 is mutated in individuals with an ataxia-telangiectasia-like disorder. Cell 1999;99:577–587. [PubMed: 10612394]

Tomita K, Matsuura A, Caspari T, Carr AM, Akamatsu Y, Iwasaki H, Mizuno K, Ohta K, Uritani M, Ushimaru T, et al. Competition between the Rad50 complex and the Ku heterodimer reveals a role for Exo1 in processing double-strand breaks but not telomeres. Mol Cell Biol 2003;23:5186–5197. [PubMed: 12861005]

Trenz K, Smith E, Smith S, Costanzo V. ATM and ATR promote Mre11 dependent restart of collapsed replication forks and prevent accumulation of DNA breaks. Embo J 2006;25:1764–1774. [PubMed: 16601701]

Trujillo KM, Yuan SS, Lee EY, Sung P. Nuclease activities in a complex of human recombination and DNA repair factors Rad50, Mre11, and p95. J Biol Chem 1998;273:21447–21450. [PubMed: 9705271]

Trujillo KM, Sung P. DNA structure-specific nuclease activities in the Saccharomyces cerevisiae Rad50/Mre11 complex. J Biol Chem 2001;276:35458–35464. [PubMed: 11454871]

Usui T, Ohta T, Oshiumi H, Tomizawa J, Ogawa H, Ogawa T. Complex formation and functional versatility of Mre11 of budding yeast in recombination. Cell 1998;95:705–716. [PubMed: 9845372]

Wen Q, Scorah J, Phear G, Rodgers G, Rodgers S, Meuth M. A Mutant Allele of MRE11 Found in Mismatch Repair Deficient Tumor Cells Suppresses the Cellular Response to DNA Replication Fork Stress in a Dominant Negative Manner. Mol Biol Cell 2008;19:1693–1705. [PubMed: 18256278]

Williams RS, Lee MS, Hau DD, Glover JN. Structural basis of phosphopeptide recongnition by the BRCT domain of BRCA1. Nat Struct Mol Biol 2004;11:519–525. [PubMed: 15133503]

Williams RS, Williams JS, Tainer JA. Mre11-Rad50-Nbs1 is a keystone complex connecting DNA repair machinery, double-strand break signaling, and the chromatin template. Biochem Cell Biol 2007;85:509–520. [PubMed: 17713585]

Wyman C, Kanaar R. DNA double-strand break repair: all's well that ends well. Annu Rev Genet 2006;40:363–383. [PubMed: 16895466]

You Z, Chahwan C, Bailis J, Hunter T, Russell P. ATM activation and its recruitment to damaged DNA require binding to the C terminus of Nbs1. Mol Cell Biol 2005;25:5363–5379. [PubMed: 15964794]

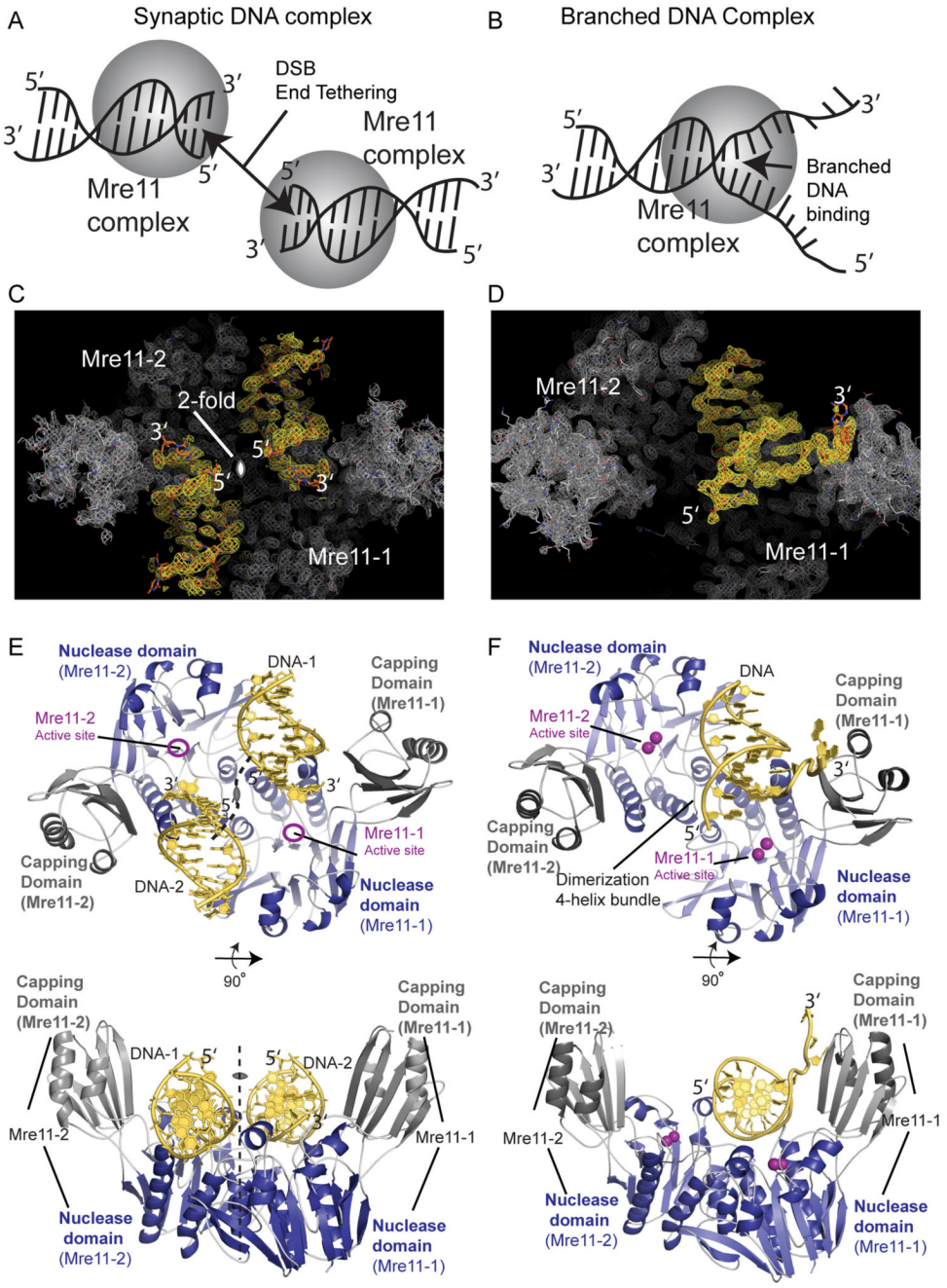

Figure 1. Mre11 X-ray Structures for Synaptic and Branched DNA Complexes

(A,B) Mre11 complex association with synaptic (A) and branched (B) DNA ends shown schematically.

(C) Synaptic DNA end complex experimental electron density. The 2.7 Å resolution composite simulated annealing 2Fo-Fc electron density map contoured at 0.8σ shows the bound DNA (yellow) overlaid upon Mre11 dimer density (grey).

(D) Branched DNA complex experimental electron density. The sigma-A weighted 2.2 Å 2Fo-Fc model phased map (calculated prior to building the DNA chain) is contoured at 1.0σ.

(E) Dimeric Mre11 can align and tether two DNA ends. Upper and lower orthogonal views show the Mre11-DNA complex for synaptic DNA ends: Mre11 fold as ribbons for helix and

beta strand and as yellow backbone tubes with planar bases for DNA. Two Mre11 subunits, which are oriented about a crystallographic two-fold axis (dotted line), bind the terminal ends of the DNA substrates (yellow).

(F) Mre11 binds the branched DNA substrate mimicking a collapsed replication fork. Upper and lower orthogonal views show Mre11-DNA binds the branched DNA substrate asymmetrically in one half of the Mre11 dimeric cleft with both Mre11 subunits contributing to binding one dsDNA. The Mre11 dimer orients around NCS related protomer contacts.

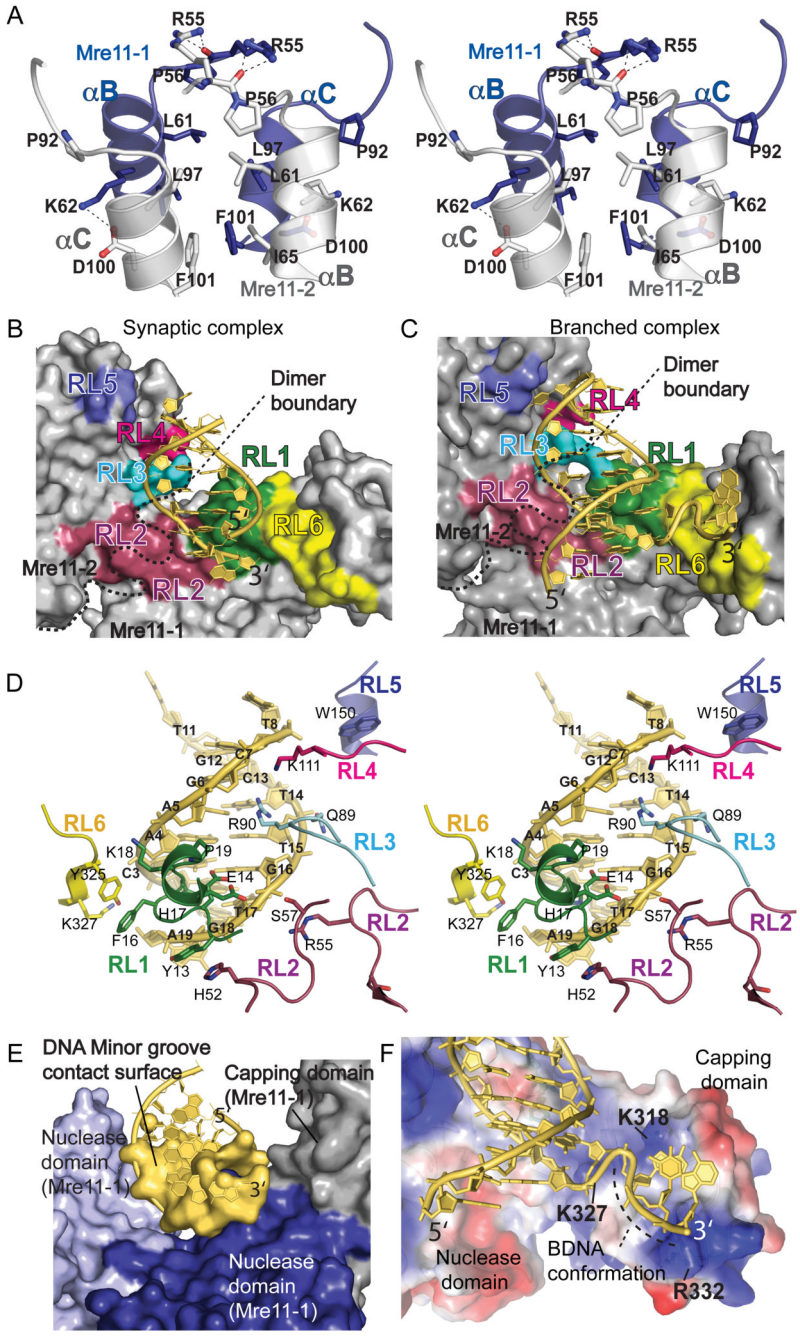

Figure 2. Mre11 Dimer-Mediated DNA Binding Interactions

(A) Mre11 homodimeric interface. Stereo view shows the Mre11-Mre11 4-helix bundle interactions at the DNA synaptic end complex crystallographic two-fold axis.

(B) Dimeric Mre11 molecular binding surface (1.4 Å probe) with dsDNA (yellow tubes, bases, and surface) for the synaptic end DNA complex, Mre11:DNA structures identify six Mre11 DNA binding motifs: recognition loops RL1 (green), RL2 (purple), RL3 (turquoise), RL4 (pink), RL5 (dark blue) and RL6 (yellow). The minor groove wedge (green) is formed from RL1 residues E14, P10 and H17 (colored molecular surfaces).

(C) Branched DNA complex with colored molecular surface for the RL1-RL6 DNA binding motif interactions.

(D) Duplex DNA contacts in the Mre11 synaptic end DNA complex. Stereo view shows all six Mre11 DNA recognition loops engage the DNA minor groove and phosphate backbone (yellow).
(E) Dimeric Mre11 molecular binding surface (1.4 Å probe) for dsDNA (yellow tubes, bases, and surface) including the roles of the two nuclease subunits (light and dark blue) and the capping domain (grey) acting in binding DNA minor groove and backbone.
(F) Nuclease domain DNA binding cleft (molecular surface colored by electrostatic potential from blue positive to red negative) showing that the branched DNA 3' tail is molded into a B-form conformation.

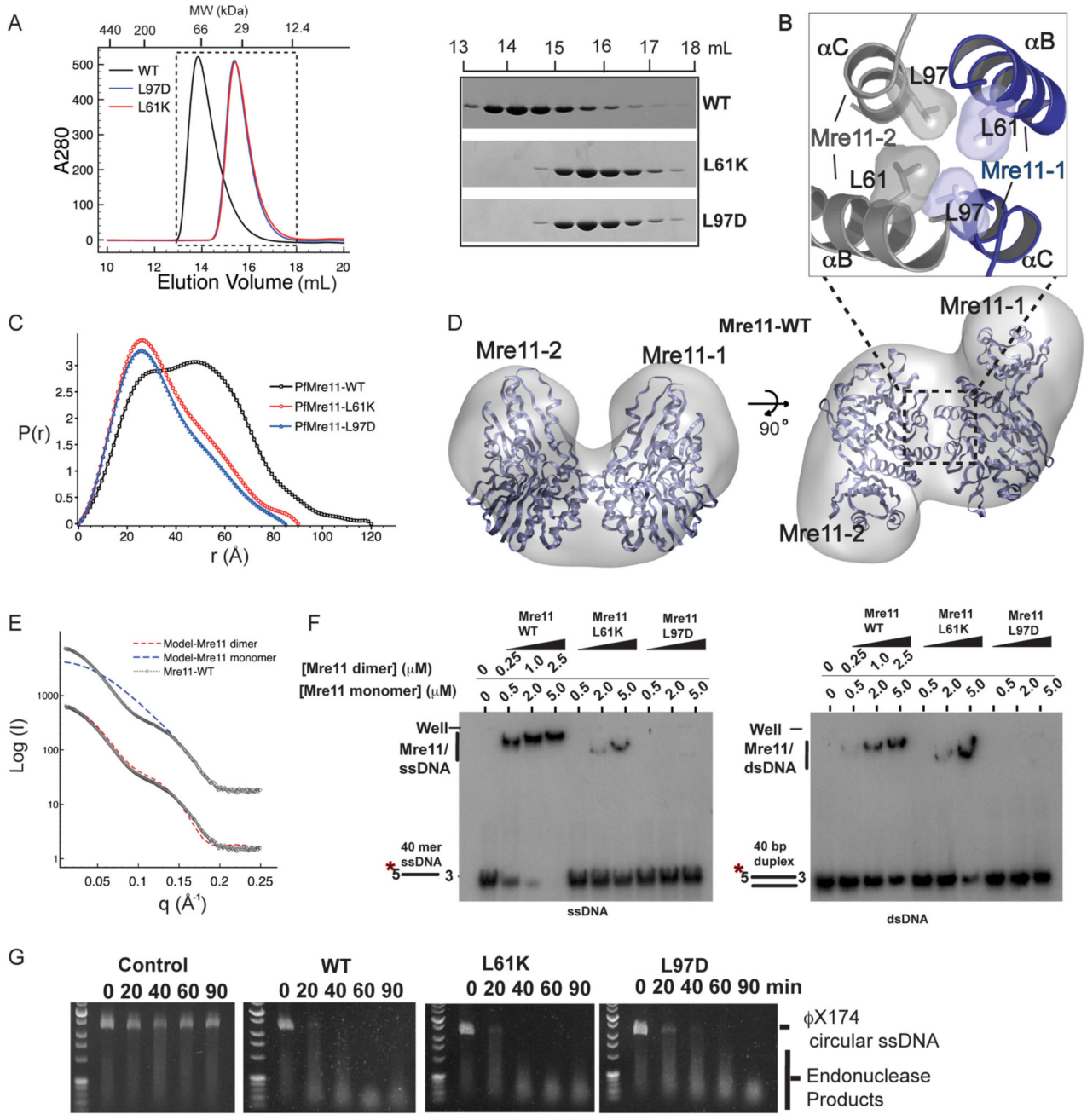

Figure 3. Mre11 Dimerization is Key to Stable DNA Binding but not Endonuclease Activity

(A) Gel Filtration analysis of Mre11 dimerization. Equivalent amounts (1.0 mg) of protein were loaded onto a Tricorn Superdex200GL (GE Amersham) column. Right - Coomassie stained SDS-PAGE of eluted fractions from the peaks between 13 mL and 18 mL.

(B) Mre11 dimer interface viewed in cross-section. Leu61 and Leu97 side-chain pairs (grey and blue subunits) pack together to form the hydrophobic core of the four-helix bundle dimer interface.

(C) Wild-type Mre11 dimer and designed mutant monomers characterized by small angle x-ray solution scattering (SAXS). SAXS electron pair distance distribution (P(r)) functions for WT Mre11 (black), Mre11-L61K (red), and Mre11-L97D.

(D) SAXS solution structure (transparent grey envelope) for Mre11 overlaid with crystallographic dimer structure (blue ribbons). Orthogonal views of an averaged GASBOR SAXS *ab initio* solution reconstruction envelope for WT Mre11 are aligned with the Mre11 dimer structure revealing that the compact dimer interface is maintained in solution.
(E) Comparison of calculated SAXS curves for Mre11 monomer (blue) and dimer (red) models with experimental scattering for PfMre11 (black) provides independent evidence that the wild type Mre11 is dimeric.
(F) EMSA DNA binding analysis of pfMre11 dimerization variants. Mre11 monomer or dimer concentrations added are shown above wells. Left panel - EMSA of Mre11 binding to 40 mer ssDNA. Right panel - EMSA of Mre11 binding to 40 bp duplex DNA.
(G) Mre11 ssDNA endonuclease activity for dimerization variants. Control shown is variant L61K assayed at 37 °C, where archaeal Mre11 nuclease activity is negligible and contaminating nucleases from *E. coli* would be active.

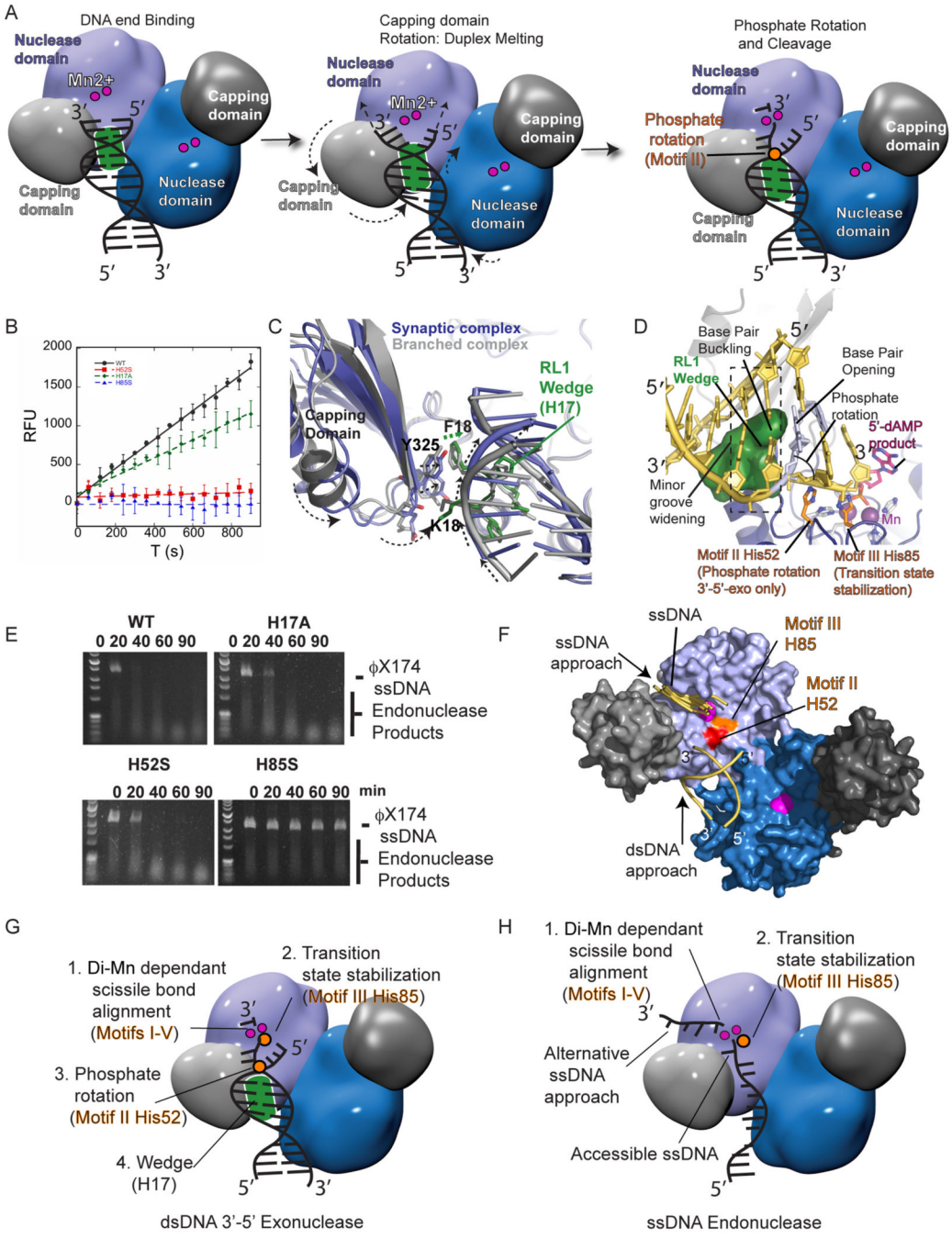

Figure 4. Differential Catalytic Requirements of Mre11 3'–5' Exonuclease and ssDNA Endonuclease Activities

(A) Proposed Mre11 3'–5' exonuclease catalytic cycle (see text for details).

(B) The 3'–5' exonuclease activity for wild-type, H17A, H52S, and H85S Mre11 proteins assayed by monitoring 2-aminopurine base release from a 2-AP containing dsDNA duplex. Error bars show +/− 1 standard deviation.

(C) Mre11 DNA complexes superimposed by alignment of the nuclease domains. Core dsDNA interacting regions for the synaptic complex (blue with green RL1 wedge residues) and branched end-binding complex (grey) are superimposed. A helical translocation of the bound

DNA is coupled to capping domain rotation. RL1 wedge His17 (Green) advances 1.8 Å into the minor groove.

(D) Structural basis for Mre11 3'–5' exonuclease reactions. The 5'-dAMP (pink) position in the exonuclease product complex (RCSB ID:1II7) and observed 3' terminus in the synaptic complex (gray) is shown relative to the proposed approach of the 3' end (yellow). 3'–5' ssDNA exonucleolytic activity requires alignment of the 3' end by His52 and His85 (orange carbon tubes with blue nitrogen atoms).

(E) ssDNA endonuclease activity for wild-type Mre11 and nuclease mechanism variants.

(F) Alternative ssDNA binding site identified by docking. All top DOT docking solutions for 3-mer ssDNA cluster to a groove at the capping to nuclease interface near the active site Mn^{2+} (pink).

(G) Minimal requirements for Mre11 3'–5' dsDNA exonuclease activity. Exonucleolytic catalysis on dsDNA substrates requires phosphate rotation via Motif II histidine to liberate the 3' terminus from duplex DNA, Mn-dependant alignment of the scissile phosphodiester bond, and stabilization of the transition state by motif III histidine.

(H) Minimial requirements for ssDNA endonuclease activity. The ssDNA backbone is inherently flexible and accessible, obviating the need for ssDNA extraction by phosphate rotation via the Motif II histidine. Mn-dependant alignment of the substrate and transition state stabilization is critical for endonucleolytic cleavage of ssDNA.

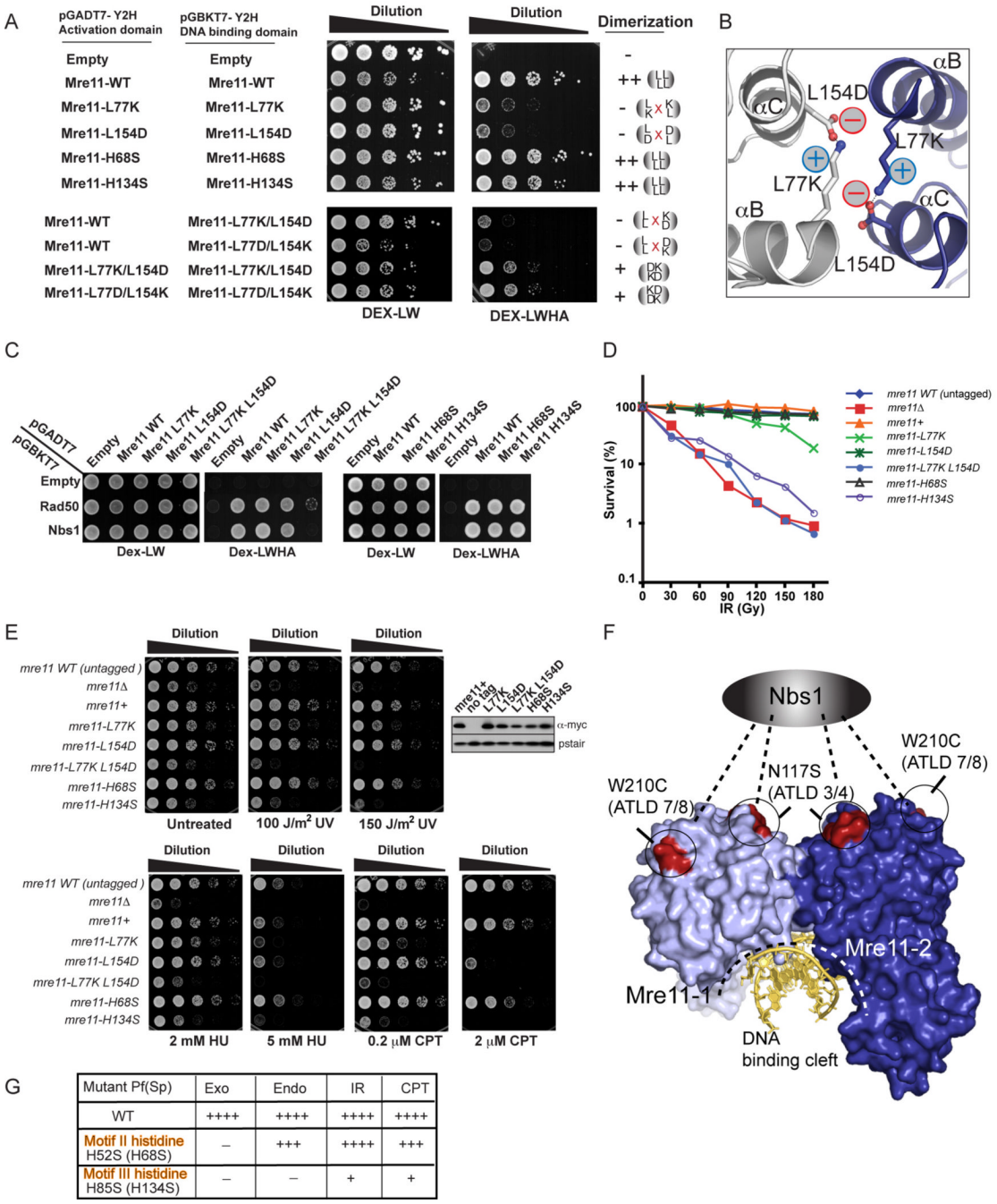

Mutant Pf(Sp)	Exo	Endo	IR	CPT
WT	++++	++++	++++	++++
Motif II histidine H52S (H68S)	–	+++	++++	+++
Motif III histidine H85S (H134S)	–	–	+	+

Figure 5. Dimerization and Nuclease Activities are Required for Mre11 complex DNA Repair Functions in *S. pombe*

(A) Mre11 self-interaction by two hybrid assays. Growth on DEX-LWHA indicates a positive two-hybrid interaction.

(B) Energy minimized model for a designed salt-bridged, reconstituted Mre11-Mre11 dimeric interface.

(C) Mre11 variant interactions with Rad50 and Nbs1 by two-hybrid analyses. Growth on Dex-LWHA indicates a positive two-hybrid interaction.

(D) Mre11 dimerization and endonuclease disruption variants are IR sensitive.

(E) CPT, HU, and UV, and show that disruption (*Mre11-L77K*) or distortion (*Mre11-L77K L154D*) of the Mre11 dimer interface or catalytic histidine mutant H134S results in clastogen sensitivity. Five-fold serial dilutions of cells on YES plates were photographed after 2–3 days growth at 30°C. Expression levels of myc-tagged wild type and mutant Mre11 proteins were determined by immuno-blotting.

(F) ATLD missense mutations W210C and N117S, which impair Nbs1 binding, cluster to a single Mre11 dimer surface opposite the DNA binding cleft.

(G) Endonuclease activity is required for efficient DSB repair in fission yeast. Mre11 catalytic activity for mutant *P. furiosus* proteins is compared to genotoxin resistance levels (++++ for wild-type to + for highly sensitive but above *mre11*$^{-}$) in fission yeast for Motif II and Motif III histidine mutant yeast strains (bracketed mutations).

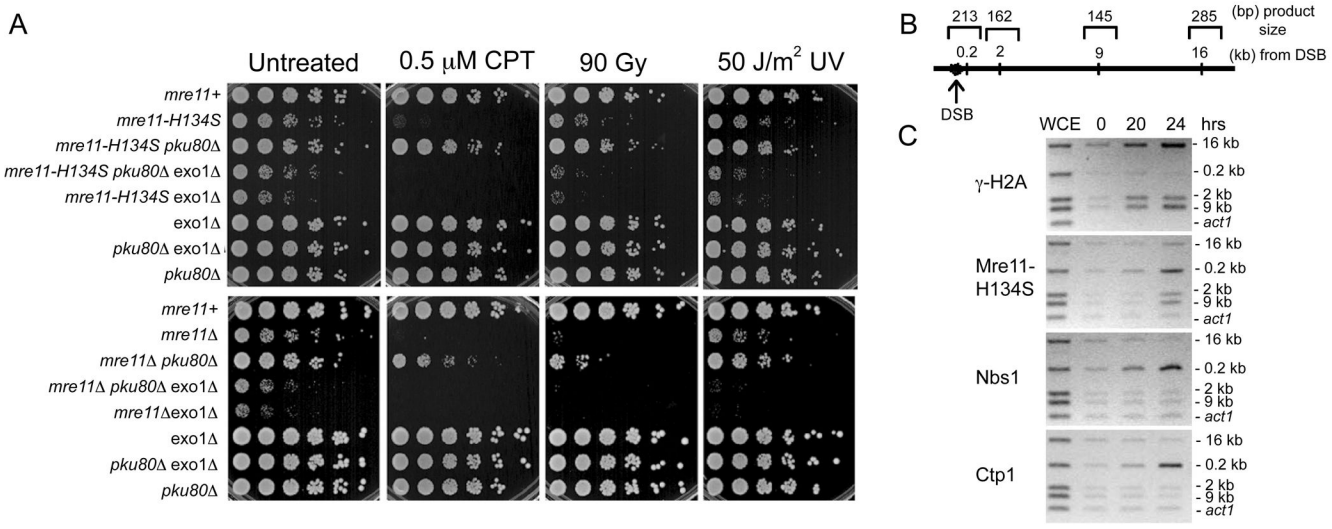

Figure 6. Exo1 Substitutes for Mre11-H134S in DSB Repair

(A) The CPT and IR survival defects of *mre11-H134S* are suppressed by eliminating Ku80 and the rescue depends on Exo1.

(B) Primers used for multiplex-PCR to amplify chromatin-immunoprecipitated DNA. Primers were designed to amplify 16kb, 0,2kb, 2kb, 9kb away from DSB and *act1* locus, and their product sizes were 285bp, 213bp, 162bp, 145bp and 121bp, respectively.

(C) MRN and Ctp1 localize to a DSB in *mre11-H134S*. ChIP assay for localization of γ-H2A, Mre11, Nbs1 and Ctp1 to a HO-induced DSB is shown for the *mre11-H134S* nuclease-deficient mutant. Samples were collected at indicated time after HO-expression. Phospho-H2A is localized at 16, 9, 2kb which is indicative of efficient HO-break formation. Mre11, Nbs1 and Ctp1 are localized specifically at 0.2kb upon DSB-formation.

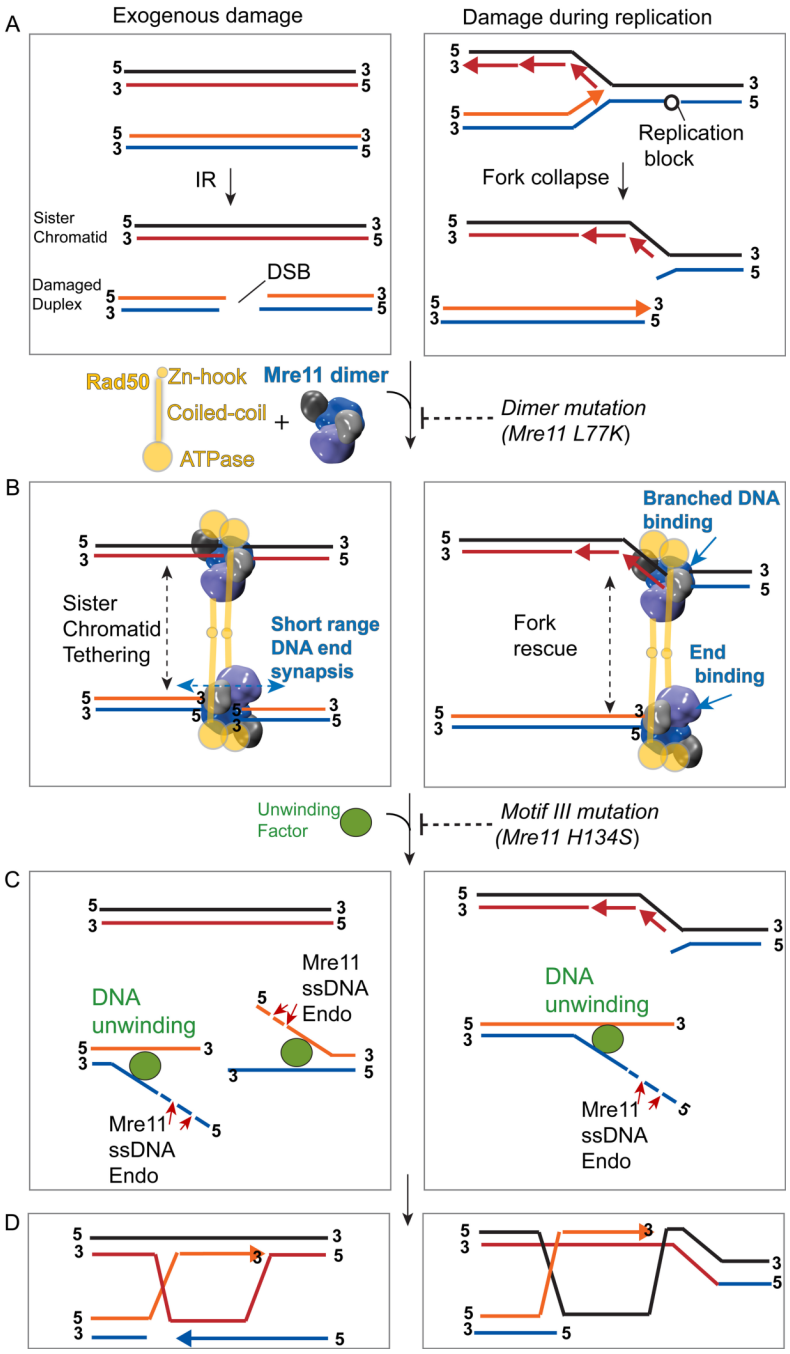

Figure 7. Mre11 Dimer Holds Together and Processes both Two-Ended Breaks from Damage and One-Ended Breaks arising during Replication

(A) DSBs arise from exogenous damage (left panels) or during replication (right panels)

(B) DNA end sensing and tethering activities are disrupted by Mre11 dimer interface mutations.

Mre11 complex scaffolding facilitates and coordinates DSB repair in response to exogenous damage or replication fork collapse by short-range Mre11 dimer-mediated DNA synapsis and by Rad50 hook-dependant long-range tethering. HR repair requires both aligning broken DSB ends, and tethering ends to a sister chromatid recombination template. Short-range synapsis links DNA ends arising from ionizing radiation in close proximity, whereas interactions through the Rad50 hook can tether the broken DNA ends to sister chromatids thereby

facilitating recombination repair. Single-end binding and branched DNA binding is appropriate for erecting structurally analogous bridging scaffolds on one-sided double strand breaks formed from collapse of replication forks.

(C) Mre11 endonuclease activity in the context of DNA unwinding is required for 5'-3' resection to generate 3' tails for strand invasion. Mre11 nuclease mutation H134S disrupts DSB processing steps for initiation of HR repair.

(D) Homologous recombination repair initiated by liberated 3' termini.